Classical and Quantum Computing near Conformality

Yannick Meurice

The University of Iowa

yannick-meurice@uiowa.edu
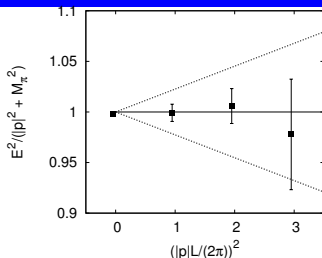
Work done in part with Alexei Bazavov, Zech Gelzer, Shan-Wen Tsai, Judah Unmuth-Yockey, Li-Ping Yang, and Jin Zhang

CERN, June 27 2016

Emergence in Lattice Gauge Theory

1. Lorentz symmetry. The lattice breaks the continuous relativistic symmetry, however for momenta small enough, we recover $E^2 = |\vec{p}|^2 + m^2$ (example in PRD 92, 014024 (2015) for $B \to \pi e \nu$)

2. Conformal symmetry. The 2D lattice $O(2)$ model has a conformal (KT, superfluid) phase reached for large enough chemical potential or hopping parameter, where the entanglement entropy scales like $(c/3)\ln(L)$ with $c \simeq 1$.

ENTANGLEMENT ENTROPY
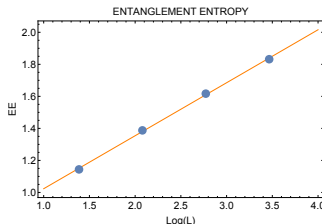
3. Local gauge symmetry. The Fermi-Hubbard model at half filling has an unexpected local symmetry (Anderson et al.). At strong coupling, there is a clear analogy with a $SU(2)$ lattice gauge theory with fermions (Fradkin et al.). See Ch. 9 of X.-G. Wen's QFT book.

Content of the talk

1. QCD motivations, overview
2. The Tensor Renormalization Group (TRG) method
   - Exact blocking formulas (spin and gauge lattice models)
   - Fixed points and exponents (Ising)
   - Chemical potential ($O(2)$, superfluid-BKT phase)
   - Entanglement entropy ($O(2)$: $c = 1$ CFT)
   - The Polyakov's loop in the Abelian Higgs model
   - The time continuum limit
3. Proposals for quantum simulators for 2D abelian models using optical lattices
4. Conclusions
5. Extra topics
   - Finite size scaling (Fisher's zeros) for spin models and SU(3) with 4 and 12 flavors
   - Emergence of local symmetries in Fermi Hubbard models

Important Lattice QCD problems/questions

- A common problem to practical lattice QCD calculations: large box size/small lattice spacing = many lattice sites.

- The problem gets more acute for many flavors with small masses (composite Higgs models?). Existence of non-trivial IR fixed points for enough flavors (e.g. $SU(3)$ with 12 massless quarks)? What are the remnants of the expected CFT on the lattice? Is there a topological picture? Again, lattices used in numerical calculations always seem too small.

- Finite density calculations: sign problem (MC calculations with complex actions are only possible if the imaginary part is small enough to be handled with reweighing).

- Real time evolution: requires detailed information about the Hamiltonian and the states which is usually not available from conventional MC simulations at Euclidean time.

Strategies

- These questions can be addressed by using two parallel and complementary approaches: renormalization group (blocking) methods and quantum simulations.

- We start with simple models and work our way up on the "lattice ladder" of models (2D Ising, 2D sigma models, 3D U(1) gauge theory , ...).

- We have made good progress with a new blocking method (TRG) for abelian models in 1+1 dimensions and hope to convince cold atom experimentalists to quantum simulate Hubbard models expected to share important features with these abelian models.

The Tensor Renormalization Group (TRG) Method

- Exact blocking (spin and gauge, PRD 88 056005)
- Applies to many lattice models: Ising model, $O(2)$ model, $O(3)$ model, Principal chiral models, Abelian and $SU(2)$ gauge theories
- Solution of sign problems (PRD 89, 016008)
- Can be checked with (worm) sampling methods (Prokofiev, Svistunov, Banerjee, Chandrasekharan, Gattringer ...)
- Critical exponents (Y.M. PRB 87, 064422, Kadanoff et al. RMP 86)
- Connects easily to the Hamiltonian picture and provides spectra
- Used to design quantum simulators: $O(2)$ model with a chemical potential (PRA 90, 063603), Abelian Higgs model (PRD 92 076003) on optical lattices
- Schwinger model: Y. Shimizu and Y. Kuramashi (PRD 90, 074503 and 014508)

Block Spining in Configuration Space is difficult!
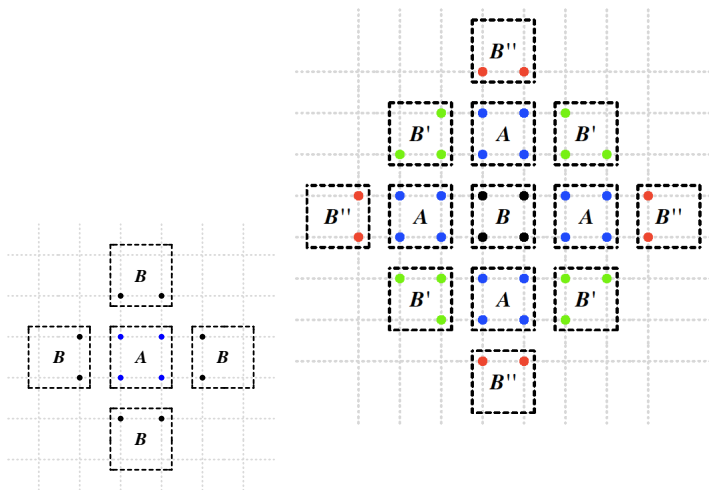
Ising 2: Step 1, Step 2, ...write a formula for the blocked Hamiltonian!

Ising model: for each link, we use the Z_2 character expansion:

$$\exp(\beta\sigma_1\sigma_2) = \cosh(\beta)(1 + \sqrt{\tanh(\beta)}\sigma_1\sqrt{\tanh(\beta)}\sigma_2) =$$
$$cosh(\beta) \sum_{n_{12}=0,1} (\sqrt{\tanh(\beta)}\sigma_1\sqrt{\tanh(\beta)}\sigma_2)^{n_{12}}.$$

Regroup the four terms involving a given spin σ_i and sum over its two values ± 1. The results can be expressed in terms of a tensor: $T^{(i)}_{xx'yy'}$ which can be visualized as a cross attached to the site i with the four legs covering half of the four links attached to i. The horizontal indices x, x' and vertical indices y, y' take the values 0 and 1 as the index n_{12}.

$$T^{(i)}_{xx'yy'} = f_x f_{x'} f_y f_{y'} \delta \left(\mathrm{mod}[x + x' + y + y', 2] \right) \ ,$$

where $f_0 = 1$ and $f_1 = \sqrt{\tanh(\beta)}$. The delta symbol is 1 if $x + x' + y + y'$ is zero modulo 2 and zero otherwise.

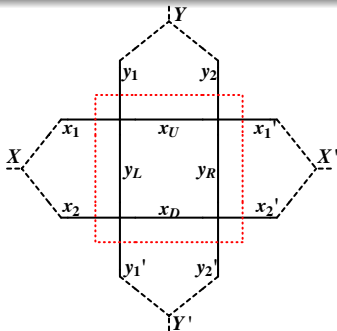## New form of the partition function:

$$Z = (\cosh(\beta))^{2V} \mathrm{Tr} \prod_i T^{(i)}_{xx'yy'}.$$

Tr means contractions (sums over 0 and 1) over the link indices.
Reproduces the closed paths of the HT expansion.

Important feature of the TRG blocking:

It separates the degrees of freedom inside the block (integrated over), from those kept to communicate with the neighboring blocks.

Graphically :
(isotropic blocking)

TRG Blocking defines a new rank-4 tensor $T'_{XX'YY'}$

Exact blocking formula (isotropic):

$$T'_{X(x_1,x_2)X'(x'_1,x'_2)Y(y_1,y_2)Y'(y'_1,y'_2)} =$$
$$\sum_{x_U,x_D,x_R,x_L} T_{x_1 x_U y_1 y_L} T_{x_U x'_1 y_2 y_R} T_{x_D x'_2 y_R y'_2} T_{x_2 x_D y_L y'_1} ,$$

where $X(x_2, x_2)$ is a notation for the product states e. g. ,
$X(0,0) = 1$, $X(1,1) = 2$, $X(1,0) = 3$, $X(0,1) = 4$.

The partition function can again be written as

$$Z = \mathrm{Tr} \prod_{2i} T'^{(2i)}_{XX'YY'} ,$$

where 2*i* denotes the sites of the coarser lattice with twice the lattice
spacing of the original lattice.

Anisotropic blocking and projection

Numerical calculations require truncations in the sum over the tensor indices. The truncation method of T. Xiang et al. (PhysRevB.86.045139) relies on an anisotropic blocking involving two sites. This provides a new rank-4 tensor:

$$M^{<ij>}_{X(x_1,x_2)X'(x_1'x_2')yy'} = \sum_{y''} T^{(i)}_{x_1,x_1',y,y''} T^{(j)}_{x_2 x_2' y'' y'} \, ,$$

which can be put in a canonical form by using a Higher Order Singular Value Decomposition defined by a unitary transformation on each of the indices. Only the d highest eigenvalues of the "metric" $G_{XX'}$

$$G_{XX'} = \sum_{X''yy'} M_{XX''yy'} M^*_{X'X''yy'}$$

are kept. This generates a new tensor with d states associated with each of the 4 indices.
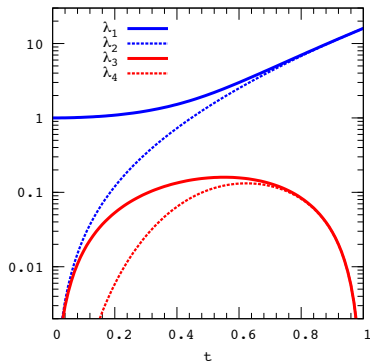
Two state approximations (2D Ising)

Figure: The four eigenvalues of $G_{XX'}$ at the first step, on a logarithmic scale, as a function of $t = th\beta$. After iterations the gap sharpens as if going to smaller t for $t < t_c$ or larger t for $t > t_c$. (YM, PRB 87, 064422)

Accurate exponents from approximate tensor renormalizations (YM, Phys. Rev. B 87, 064422 2013)

- For the Ising model on square lattice, several truncation methods sharply singles out a surprisingly small subspace of dimension two.

- In the two states limit, the transformation can be handled analytically yielding a value 0.964 for the critical exponent ν much closer to the exact value 1 than 1.338 obtained in Migdal-Kadanoff approximations. Alternative blocking procedures that preserve the isotropy can improve the accuracy to $\nu = 0.987$ and 0.993 respectively.

- Two states for 3D Ising: $\nu = 0.74$ (not so good).

- Few states improvement not well-understood.

More than two states

When a few more states are added, the quality of the approximation does not immediately improve. One first observes oscillations, false bifurcations, approximate degeneracies. Same observations were made by Leo Kadanoff (1937-2015) and collaborators.
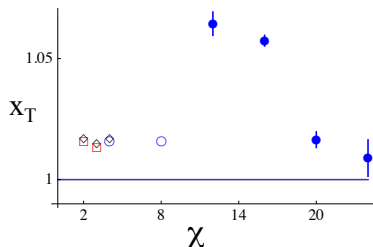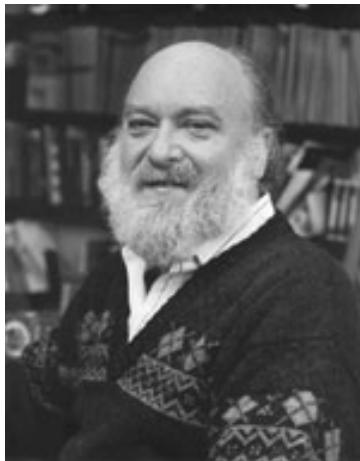

Figure: Thermal x-value $1/\nu$ versus the truncation size χ in various calculations summarized in by Efi Efrati, Zhe Wang, Amy Kolan, Leo P. Kadanoff, Rev. Mod. Phys. 86, 647 May 2014

Leo Kadanoff (1937-2015)

Kaufman exact expression of the transfer matrix for Ising 2 and TRG recursion (Y. M. work in progress)

- For a finite spatial size N_x, Kaufman uses a Clifford algebra with $2 * N_x$ gamma-matrices (2^{N_x} dimensional matrices). The transfer Matrix is a representation of product of rotations in $2N_x$ dimensions which can be diagonalized (Phys. Rev. 76, 1232 (1949)).

- "Chirality": L-R states ($\gamma_5 \rightarrow \Gamma_1 \Gamma_2 \ldots \Gamma_{2N_x}$) is even-odd in TRG

- In progress: exact Grassmann representation of the transfer matrix with recursion relations, ...

- CFT at β_c: is there a remnant of $z \rightarrow -1/z$ transformation on a finite lattice? Can we obtain the continuum expression of Itzykson et al. for the correlation functions (in terms of modular functions, see Ph. de Forcrand and O. Akerlund 1410.1178) from the fixed point? S. Smirnov work on CFT for the critical Ising model, Field medal 2010, may help.

$$Z = \int \prod_{(x,t)} \frac{d\theta_{(x,t)}}{2\pi} e^{-S}.$$

$$\begin{aligned}
S = & - \beta_{\hat{t}} \sum_{(x,t)} \cos(\theta_{(x,t+1)} - \theta_{(x,t)} - i\mu) \\
& - \beta_{\hat{x}} \sum_{(x,t)} \cos(\theta_{(x+1,t)} - \theta_{(x,t)}).
\end{aligned}$$

$$\begin{aligned}
Z = & \sum_{\{n\}} \prod_{(x,t)} I_{n_{(x,t),\hat{x}}}(\beta_{\hat{x}}) I_{n_{(x,t),\hat{t}}}(\beta_{\hat{t}}) e^{\mu n_{(x,t),\hat{t}}} \\
& \times \delta_{n_{(x-1,t),\hat{x}}+n_{(x,t-1),\hat{t}},n_{(x,t),\hat{x}}+n_{(x,t),\hat{t}}}.
\end{aligned}$$

For real μ the action is complex, $\beta = 1/g^2$

Worm configurations
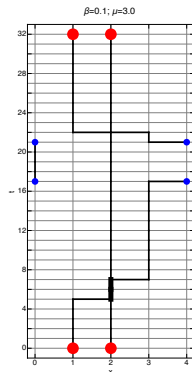
Figure: Allowed configuration of $\{n\}$ for a 4 by 32 lattice. The uncovered links on the grid have $n=0$, the more pronounced dark lines have $|n|=1$ and the wider lines have $n=2$. The dots need to be identified periodically. The time slice 5, represents a transition between $|1100\rangle$ and $|0200\rangle$. Statitical sampling of these configurations (worm algorithm) has been used to check the TRG calculations.

TRG approach of the transfer matrix

The partition function can be expressed in terms of a transfer matrix:

$$Z = \operatorname{Tr} \mathbb{T}^{L_t} .$$

The matrix elements of $\mathbb{T}$ can be expressed as a product of tensors associated with the sites of a time slice (fixed t) and traced over the space indices (PhysRevA.90.063603)

$$\mathbb{T}_{(n_1, n_2, \ldots n_{L_x})(n_1', n_2' \ldots n_{L_x}')} = \sum_{\tilde{n}_1 \tilde{n}_2 \ldots \tilde{n}_{L_x}} T^{(1,t)}_{\tilde{n}_{L_x} \tilde{n}_1 n_1 n_1'} T^{(2,t)}_{\tilde{n}_1 \tilde{n}_2 n_2 n_2' \ldots} \cdots T^{(L_x,t)}_{\tilde{n}_{L_x-1} \tilde{n}_{L_x} n_{L_x} n_{L_x}'}$$

with

$$T^{(x,t)}_{\tilde{n}_{x-1} \tilde{n}_x n_x n_x'} = \sqrt{I_{n_x}(\beta_{\hat{t}}) I_{n_x'}(\beta_{\hat{t}}) I_{\tilde{n}_{x-1}}(\beta_{\hat{x}}) I_{\tilde{n}_x}(\beta_{\hat{x}}) \mathrm{e}^{(\mu(n_x + n_x'))}} \delta_{\tilde{n}_{x-1} + n_x, \tilde{n}_x + n_x'}$$

The Kronecker delta function reflects the existence of a conserved current, a good quantum number ("particle number").

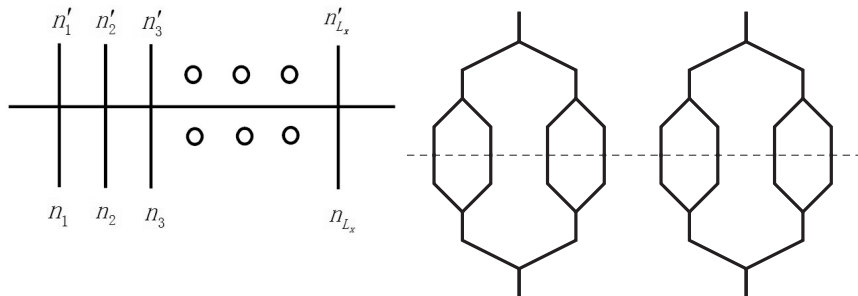# Coarse-graining of the transfer matrix

Figure: Graphical representation of the transfer matrix (left) and its successive coarse graining (right). See PRD 88 056005 and PRA 90, 063603 for explicit formulas.
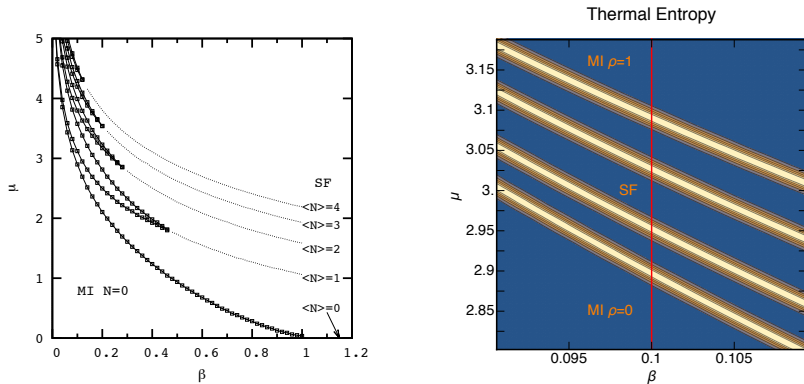
Phase diagram

Figure: Mott Insulating "tongues" and Thermal entropy in a small region of the $\beta - \mu$ plane. Intensity plot for the thermal entropy of the classical XY model on a 4×128 lattice in the β-μ plane. The dark (blue) regions are close to zero and the light (yellow ochre) regions peak near $\ln 2$ (level crossing).
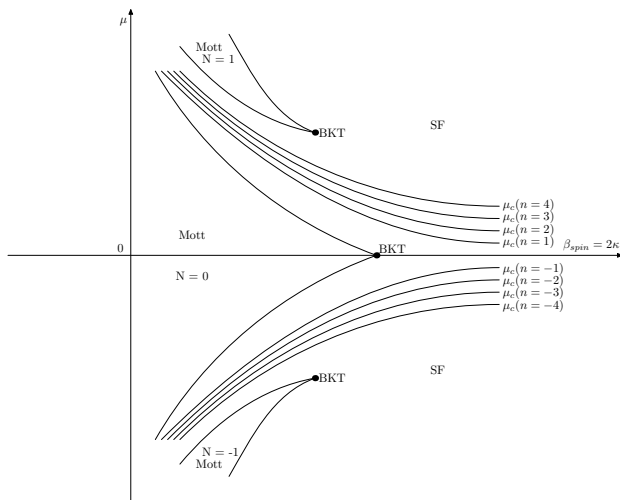
O(2) Gap ($N_x = 4$ illustration)

Figure: Schematic description of the jumps in thermal entropy (level crossing) for $N_x = 4$ in the $\beta - \mu$ plane.

Entanglement entropy S_E (PRE 93, 012138 (2016))

We consider the subdivision of AB into A and B (two halves in our calculation) as a subdivision of the spatial indices.

$$\hat{\rho}_A \equiv \mathrm{Tr}_B \hat{\rho}_{AB}; \quad S_E = -\sum_i \rho_{A_i} \ln(\rho_{A_i}). \tag{1}$$

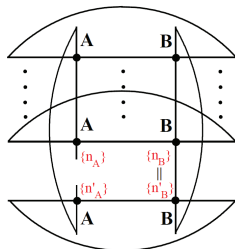We use blocking methods until A and B are each reduced to a single site.

Figure: The horizontal lines represent the traces on the space indices. There are L_t of them, the missing ones being represented by dots. The two vertical lines represent the traces over the blocked time indices in A and B.
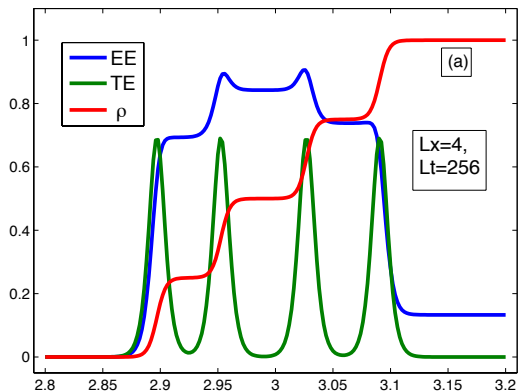
The fine structure for $L_x = 4$, $L_t = 256$

Figure: Entanglement entropy (EE, blue), thermal entropy (TE, green) and particle density ρ (red) versus the chemical potential μ. The thermal entropy has $L_x = 4$ peaks culminating near $\ln 2 \simeq 0.69$; ρ goes from 0 to 1 in $L_x = 4$ steps and the entanglement entropy has an approximate mirror symmetry near half fillings where it peaks. ($L_x = N_s$ in other figures).
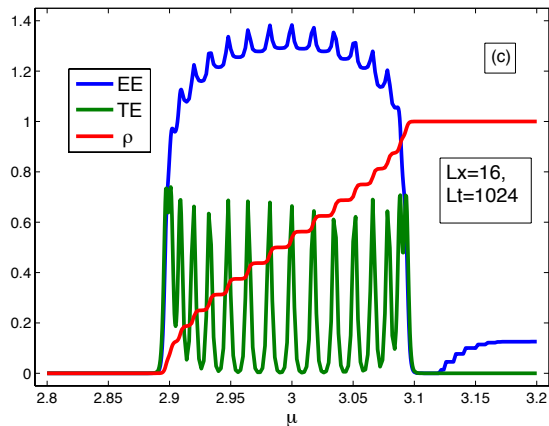
Similar features for $L_x = 16$ with $L_t = 1024$

Figure: Entanglement entropy (EE, blue), thermal entropy (TE, green) and particle density ρ (red). The thermal entropy has $L_x = 16$ peaks culminating near $\ln 2 \simeq 0.69$; ρ goes from 0 to 1 in $L_x = 16$ steps and the entanglement entropy has an approximate mirror symmetry near half fillings where it peaks.
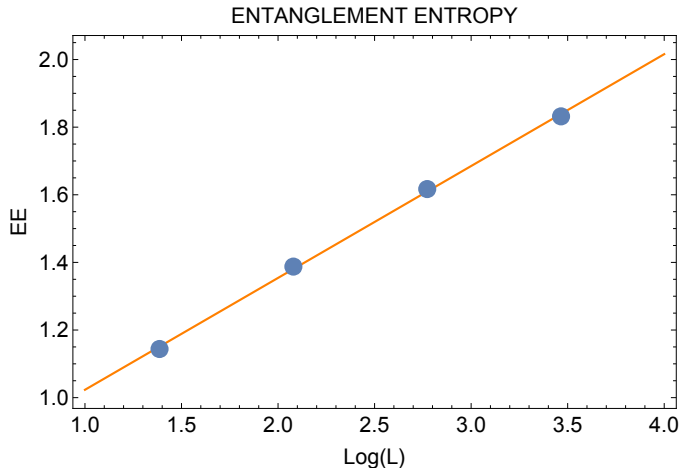
Cardy scaling : c=1?

ENTANGLEMENT ENTROPY

Figure: Entanglement entropy for $O(2)$, $\mu = 0$, $\beta_{spin} = 1.2$. The fit is 0.692 + 0.331 Log(L). Cardy CFT prediction is $cst. + (c/3)Log(L)$. Data from Li-Ping Yang.

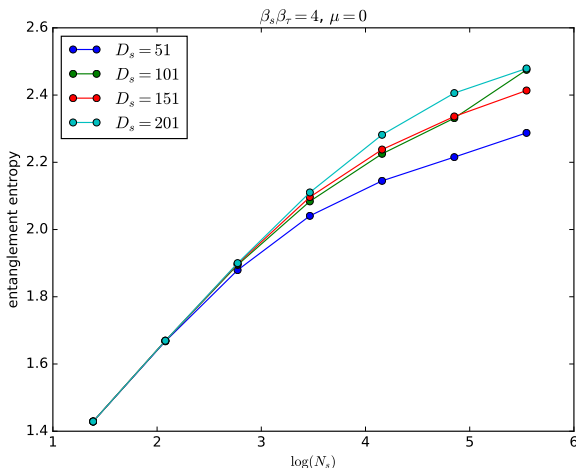# Larger N_s requires larger D_{bound}

Figure: Entanglement entropy for $O(2)$, $\mu = 0$. Data from J. Unmuth-Yockey.

The Abelian Higgs model on a 1+1 space-time lattice

a.k.a. lattice scalar electrodynamics. Field content:
- Complex (charged) scalar field $\phi_x = |\phi_x|e^{i\theta_x}$ on space-time sites x
- Abelian gauge fields $U_{x,\mu} = \exp iA_\mu(x)$ on the links from x to $x + \hat{\mu}$
- $F_{\mu\nu}$ appears when taking products of U's around an elementary square (plaquette) in the $\mu\nu$ plane
- Notation for the plaquette: $U_{x,\mu\nu} = e^{i(A(x)_\mu + A(x+\hat{\mu})_\nu - A(x+\hat{\nu})_\mu - A(x)_\nu)}$
- $\beta_{pl.} = 1/e^2$ and κ is the hopping coefficient

$$
\begin{aligned}
S \;=\; & -\beta_{pl.} \sum_x \sum_{\nu < \mu} \mathrm{ReTr}\,[U_{x,\mu\nu}] + \lambda \sum_x \left(\phi_x^\dagger \phi_x - 1\right)^2 + \sum_x \phi_x^\dagger \phi_x \\
& - \kappa \sum_x \sum_{\nu=1}^{d} \left[e^{\mu_{ch.}\,\delta(\nu,t)} \phi_x^\dagger U_{x,\nu} \phi_{x+\hat{\nu}} + e^{-\mu_{ch.}\,\delta(\nu,t)} \phi_{x+\hat{\nu}}^\dagger U_{x,\nu}^\dagger \phi_x \right].
\end{aligned}
$$

$$
Z = \int D\phi^\dagger D\phi\, DU\, e^{-S}
$$

Unlike other approaches (Reznik, Zohar, Cirac, Lewenstein, Kuno,....) we will not try to implement the gauge field on the optical lattice.

Gauge-invariant effective action

At the lowest order of the strong-coupling expansion we set $\beta_{pl.} = 0$ (we neglect the plaquette interaction) and carry out the DU (gauge) integration. The effect of the plaquette can be restored order by order. We obtain an effective theory

$$Z = \int D\phi^\dagger D\phi DU e^{-S} = \int DM e^{-S_{eff.}(M)}$$

for the composite (gauge invariant) field $M_x = \phi_x^\dagger \phi_x$ with an effective action

$$S_{eff} = \sum_{<xy>} (-\kappa^2 M_x M_y + (1/4)\kappa^4 (M_x M_y)^2)$$

$$-2\kappa^4 (I_1(\beta_{pl.})/I_0(\beta_{pl.})) \sum_{pl(xyzw)} M_x M_y M_z M_w + O(\kappa^6)$$

For a similar approach with fermions see "Lattice gauge theory without link variables" by H. Vairinhos and P. de Forcrand JHEP 1412 038.

Monte Carlo checks of the hopping expansion and plaquette corrections for $L_\phi = \langle \mathrm{Re}\{\phi_x^\dagger U_{x,\hat{\nu}} \phi_{x+\hat{\nu}}\}\rangle$
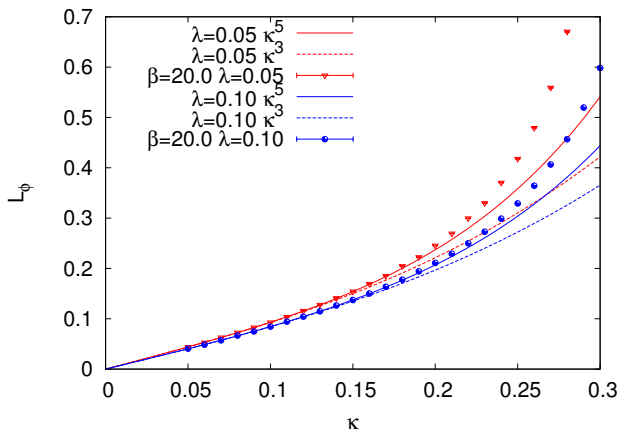

Figure: L_ϕ at $\beta_{pl} = 20$ for $\lambda = 0.05$ and $\lambda = 0.1$ as function of κ compared with the hopping expansion at $\beta_{pl} = \infty$ at $O(\kappa^3)$ and $O(\kappa^5)$.

The large λ limit

$\lambda \to \infty$, $|\phi_x|$ is frozen to 1, or in other words, the Brout-Englert-Higgs mode becomes infinitely massive.

We are then left with compact variables of integration in the original formulation (θ_x and $A_{x,\hat{\nu}}$) and the Fourier expansions

$exp[2\kappa_{\hat{\nu}} cos(\theta_{x+\hat{\nu}} - \theta_x + A_{x,\hat{\nu}})] = \sum_{n=-\infty}^{\infty} I_n(2\kappa_{\hat{\nu}}) exp(\imath n(\theta_{x+\hat{\nu}} - \theta_x + A_{x,\hat{\nu}}))$

leads to expressions of the partition function in terms of discrete sums.

We use the following definitions:

$t_n(z) \equiv I_n(z)/I_0(z)$

$t_n(0) = \delta_{n,0}$.

For z non zero and finite, we have $1 > t_0(z) > t_1(z) > t_2(z) > \cdots > 0$

In addition for sufficiently large z,

$t_n(z) \simeq 1 - n^2/(2z)$

Tensor Renormalization Group formulation

As in PRD.88.056005 and PRD.92.076003, we attach a $B^{(\square)}$ tensor to every plaquette

$$B^{(\square)}_{m_1 m_2 m_3 m_4}$$
$$= \begin{cases} t_{m_\square}(\beta_{pl}), & \text{if } m_1 = m_2 = m_3 = m_4 = m_\square \\ 0, & \text{otherwise.} \end{cases}$$

a $A^{(s)}$ tensor to the horizontal links

$$A^{(s)}_{m_{up} m_{down}} = t_{|m_{down} - m_{up}|}(2\kappa_s),$$

and a $A^{(\tau)}$ tensor to the vertical links

$$A^{(\tau)}_{m_{left} m_{right}} = t_{|m_{left} - m_{right}|}(2\kappa_\tau)\, e^\mu.$$

The quantum numbers on the links are completely determined by the quantum numbers on the plaquettes

$Z = Tr[\prod T]$

$$Z = (I_0(\beta_{pl})I_0(2\kappa_s)I_0(2\kappa_\tau))^V \times$$

$$\mathrm{Tr}\left[\prod_{h,v,\square} A^{(s)}_{m_{up}m_{down}} A^{(\tau)}_{m_{right}m_{left}} B^{(\square)}_{m_1 m_2 m_3 m_4}\right] \propto \mathrm{Tr}(\sqrt{\mathbb{B}}\mathbb{A}\sqrt{\mathbb{B}})^{N_\tau}.$$

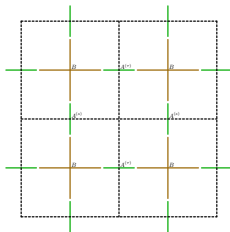The traces are performed by contracting the indices as shown

Figure: The basic B and A tensors (in brown and green, respectively, colors online). The $A^{(s)}$ are associated with the vertical tensors, and the horizontal (spatial) links of the lattice. The $A^{(\tau)}$ are associated with the horizontal tensors, and the vertical (temporal) links of the lattice.

Remarks

- The plaquette quantum numbers are the dual variables
- If we impose periodic boundary conditions on the plaquettes, we can only have neutral states (Gauss law)
- We will probe the charged sector by introducing Polyakov loops
- For related questions in QED, see arXiv:1509.01636, "Charged hadrons in local finite-volume QED+QCD with C* boundary conditions" by Biagio Lucini, Agostino Patella, Alberto Ramos, and Nazario Tantalo

Polyakov loop, a Wilson line wrapping around the Euclidean time direction: $\langle P_i \rangle = \langle \prod_j U_{(i,j),\tau} \rangle$; the order parameter for deconfinement.
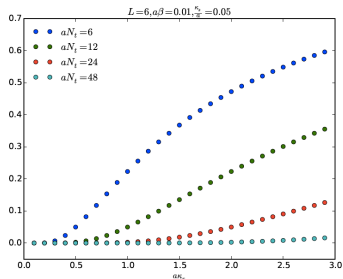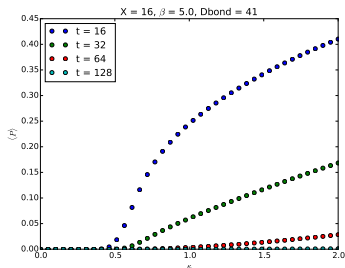
With spatial periodic boundary condition, the insertion of the Polyakov loop (red) forces the presence of a scalar current (green) in the opposite direction (left) or another Polyakov loop (right).
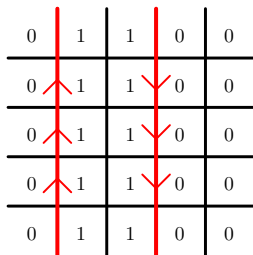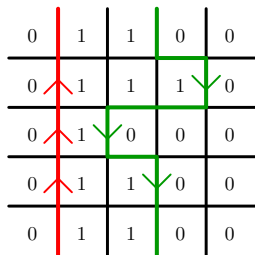
In the Hamiltonian formulation, we add $-\frac{\tilde{Y}}{2}(2(\bar{L}_{i^\star}^z - \bar{L}_{(i^\star+1)}^z) - 1)$ to H.

Polyakov loop for (1+1)D Abelian Higgs model using the TRG method (Left, Judah Unmuth-Yockey) and the Hamiltonian method (Right, Jin Zhang). Using logarithmic resolution, there is no sharp transition on the left (only exponential decay due to the gauge fields).
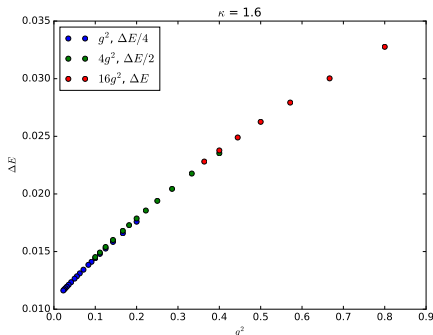
Data collapse for Polyakov loop

Guesses: $-\ln(P) \simeq C + N_\tau(\Delta E)$; $\Delta E \simeq A/N_s + Bg^2 N_s + ...$);
Data Collapse: $N_s \Delta E = F(g^2 N_s^2)$?
Recent numerical calculations by J. Unmuth-Yockey give support to
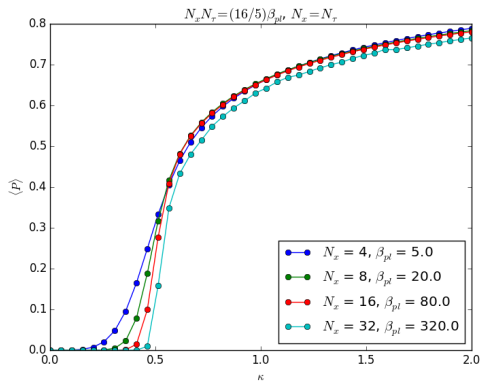this idea

Data collapse for Polyakov loop II

$$N_x N_\tau = (16/5)\beta_{pl}, \ N_x = N_\tau$$

Legend:
- $N_x = 4, \ \beta_{pl} = 5.0$
- $N_x = 8, \ \beta_{pl} = 20.0$
- $N_x = 16, \ \beta_{pl} = 80.0$
- $N_x = 32, \ \beta_{pl} = 320.0$

Figure: The increase in sharpness with volume makes it look like an order parameter. Numerical calculations by J. Unmuth-Yockey.

The time continuum limit and the energy spectrum

In the limit $\kappa_s = 0$, and if *both* κ_τ and β_{pl} become large, at leading order in the inverse of these large parameters, the eigenvalues of $\mathbb{T}$ are

$$\lambda_{(m_1, m_2, \ldots m_{N_s})} =$$
$$1 - \frac{1}{2}[(\frac{1}{\beta_{pl}}(m_1^2 + m_2^2 + \cdots + m_{N_s}^2) +$$
$$\frac{1}{2\kappa_\tau}(m_1^2 + (m_2 - m_1)^2 + \ldots$$
$$\cdots + (m_{N_s} - m_{N_s-1})^2 + m_{N_s}^2)]$$

In the case $1 << \beta_{pl} << \kappa_\tau$, we set the scale with the (large) gap energy $\tilde{U}_g \equiv 1/a\beta_{pl}$.

For $1 << \kappa_\tau << \beta_{pl}$, we tend to have strings of constant m but for large volume, the plaquette energy can take over (confinement).

The Hamiltonian for $1 << \beta_{pl} << \kappa_\tau$ and $m = 0, \pm 1$

We now use the spin-1 approximation ($m = 0, \pm 1$ or $n = 0, \pm 1$) to discuss the two cases.

For $1 << \beta_{pl} << \kappa_\tau$, We use the notation $\bar{L}^x_{(i)}$ to denote the first generator of the spin-1 rotation algebra at the site (i). The notation $\bar{L}$ is used to emphasize that the spin is related to the m quantum numbers attached to the plaquettes, not to the charges n on the time links.

We define $\tilde{Y} \equiv (\beta_{pl}/(2\kappa_\tau))\tilde{U}_g$ and $\tilde{X} \equiv (\beta_{pl}\kappa_s\sqrt{2})\tilde{U}_g$ which are the (small) energy scales. The final form of the Hamiltonian $\bar{H}$ for $1 << \beta_{pl} << \kappa_\tau$ is

$$\bar{H} = \frac{\tilde{U}_g}{2} \sum_i \left(\bar{L}^z_{(i)} \right)^2 +$$

$$\frac{\tilde{Y}}{2} \sum_i (\bar{L}^z_{(i)} - \bar{L}^z_{(i+1)})^2 - \tilde{X} \sum_i \bar{L}^x_{(i)} .$$

In the limit $\beta_{pl.} \to \infty$, $\lambda \to \infty$, we recover the Hamiltonian for the spin-1 approximation of the $O(2)$ model:

$$
\hat{H} = \frac{\tilde{U}}{2} \sum_i \left(\hat{L}^z_{(i)} \right)^2
$$
$$
- \tilde{\mu} \sum_i \hat{L}^z_{(i)} - \frac{\tilde{J}}{4} \sum_i \left(\hat{L}^+_{(i)} \hat{L}^-_{(i+1)} + \hat{L}^-_{(i)} \hat{L}^+_{(i+1)} \right) ,
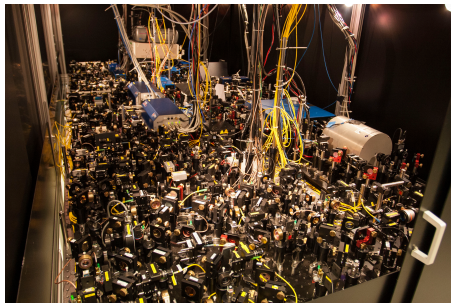$$

with the now dimensionful quantities

$$
\tilde{U} \equiv \frac{1}{2\kappa_\tau a}, \ \tilde{\mu} \equiv \frac{\mu}{a}, \ \tilde{J} \equiv \frac{2\kappa_s}{a},
$$

and a the time lattice spacing.
The operators $\hat{L}^z_{(i)}$ are associated with the time links.

Can lattice gauge theorists learn about Quantum Chromodynamics (QCD) at finite density and real time from optical lattice experiments?

The Fermilab Lattice Gauge Theory cluster (left); An optical lattice experiment (once used to observe a "Higgs mode") at MPQ (right)

Quantum Simulators

- No sign problems
- Real time evolution
- So far the linear sizes are of order 100-200 and are expected to reach 1000 soon.
- Can we do interesting experiments with small lattices?
- Finite temperature at infinite size (Euclidean time)$\sim$ finite size at zero temperature (experiment)?
- Many interesting proposals based on the Kogut-Susskind Hamiltonian and quantum rotors (Reznik, Zohar, Cirac, Wiese, Lewenstein, Kuno,....).
- Our approach is based on the tensor formulation of lattice gauge theory and is manifestly gauge invariant.
- So far, the remarkable theory-experiment reached for the Bose-Hubbard model is just a source of inspiration in the context of lattice gauge theory and a proof of principle is needed.

Quantum simulators: main message

- We have reformulated the lattice Abelian Higgs model (scalar QED) in 1 space + 1 time dimension using the Tensor Renormalization Group method

- The reformulation is gauge invariant and connects smoothly the classical Lagrangian formulation used by lattice gauge theorists and the quantum Hamiltonian method used in condensed matter

- Despite its simplicity, the model has a rich behavior (entanglement entropy scaling like in Conformal Field Theory in the weak gauge coupling limit, deconfinement at finite volume)

- We propose to use Bose-Hubbard (BH) Hamiltonians with two species as quantum simulators. Using degenerate perturbation theory, we obtain effective Hamiltonians resembling those relevant for the Abelian Higgs model

- We would like to find realistic ways to implement these BH Hamiltonians on optical lattices

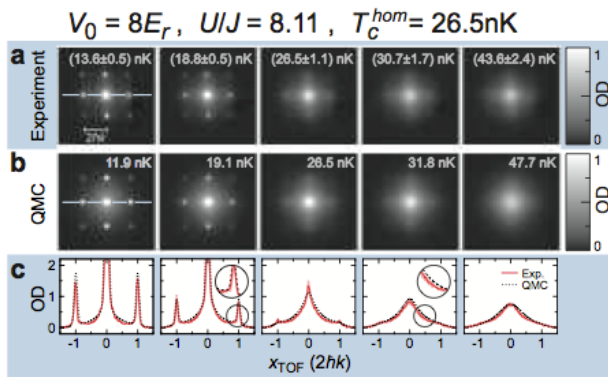# The (high) standards: Quantum Monte Carlo vs. Experiment for the Bose-Hubbard model

Figure: From S. Trotzky, L. Pollet, F. Gerbier, U. Schnorrberger, I. Bloch, N.V. Prokof'ev, B. Svistunov, M. Troyer Nature Phys. 6, 998-1004 (2010)

Two species Bose-Hubbard (PRD 92 076003)

The two-species Bose-Hubbard Hamiltonian ($\alpha = a, b$ indicates two different species, respectively) on square optical lattice reads

$$
\begin{aligned}
\mathcal{H} \quad &= -\sum_{\langle ij \rangle}(t_a a_i^\dagger a_j + t_b b_i^\dagger b_j + h.c.) - \sum_{i,\alpha}(\mu + \Delta_\alpha)n_i^\alpha \\
&+ \sum_{i,\alpha}\frac{U_\alpha}{2}n_i^\alpha(n_i^\alpha - 1) + W\sum_i n_i^a n_i^b + \sum_{\langle ij \rangle \alpha}V_\alpha n_i^\alpha n_j^\alpha \\
&- (t_{ab}/2)\sum_i (a_i^\dagger b_i + b_i^\dagger a_i)
\end{aligned}
$$

with $n_i^a = a_i^\dagger a_i$ and $n_i^b = b_i^\dagger b_i$.

In the limit where $U_a = U_b = U$ and W and $\mu_{a+b} = (3/2)U$ much larger than any other energy scale, we have the condition $n_i^a + n_i^b = 2$ for the low energy sector. The three states $|2, 0\rangle$, $|1, 1\rangle$ and $|0, 2\rangle$ satisfy this condition and correspond to the three states of the spin-1 projection considered above.

$$
\begin{aligned}
\mathcal{H}_{eff} &= (\frac{V_a}{2} - \frac{t_a^2}{U_0} + \frac{V_b}{2} - \frac{t_b^2}{U_0}) \sum_{\langle ij \rangle} L_i^z L_j^z \\
&+ \frac{-t_a t_b}{U_0} \sum_{\langle ij \rangle} (L_i^+ L_j^- + L_i^- L_j^+) + (U_0 - W) \sum_i (L_i^z)^2 \\
&+ [(\frac{pn}{2} V_a + \Delta_a - \frac{p(n+1)t_a^2}{U_0}) - (\frac{pn}{2} V_b \\
&+ \Delta_b - \frac{p(n+1)t_b^2}{U_0})] \sum_i L_i^z - t_{ab} \sum_i L_{(i)}^x
\end{aligned}
$$

where p is the number of neighbors and n is the occupation ($p = 2$, $n = 2$ in the case under consideration). $\hat{L}$ is the angular momentum operator in representation $n/2$.

Matching the O(2) and BH spectra for large *U*

Matching: with the *O*(2) model, we need to tune the hopping amplitude as $t_\alpha = \sqrt{V_\alpha U/2}$ and have $\tilde{J} = 4\sqrt{V_a V_b}$, $\tilde{U} = 2(U - W)$, and $\tilde{\mu} = -(\Delta_a - V_a) + (\Delta_b - V_b)$.
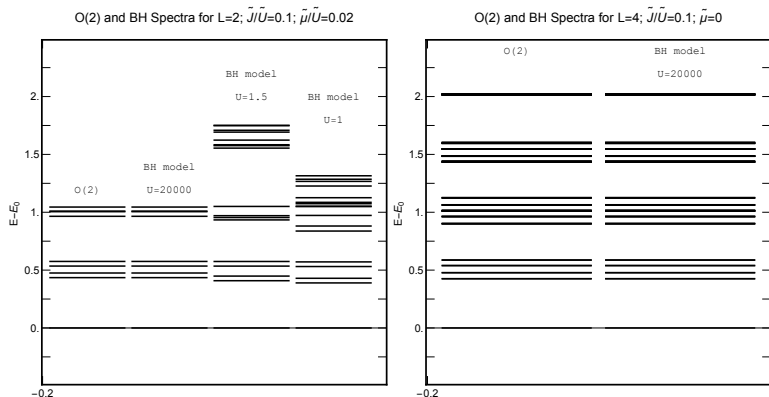

Figure: O(2) and Bose-Hubbard spectra for L=2 (left) and L=4 (right).

Optical lattice implementation (PRA 90 06303)

- The two-species: ^{87}Rb and ^{41}K Bose-Bose mixture where an interspecies Feshbach resonance is accessible (W).
- Species-dependent optical lattice are used in boson systems, which allows hopping amplitude of individual species to be tuned to desired values.
- The extended repulsion, V_α, is present and small when we consider Wannier gaussian wave functions sitting on nearby lattice sites (Mazzarella et al. 2006)
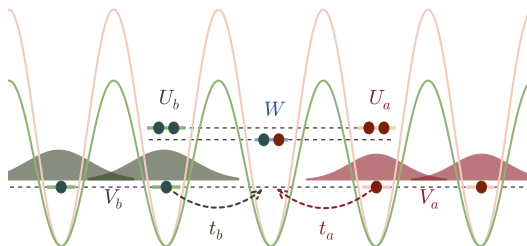
Matching Abelian Higgs model and BH spectra

Matching: $t_a = t_b = 0$, $V_a = V_b = -\tilde{Y}/2$, $t_{ab} = \tilde{X}$,
$\tilde{U}_p = 2(U - W + 2V_{a(b)})$, $\Delta_{a(b)} = -2V_{a(b)}$.
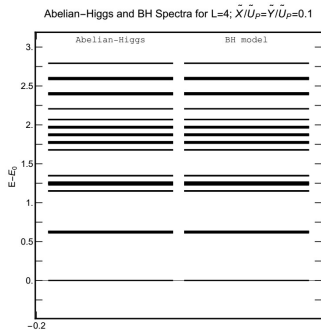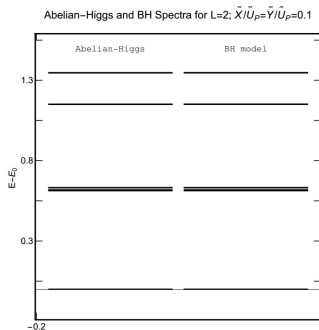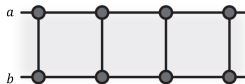
Optical lattice implementation

- Ladder structure

Figure: A ladder structure with a and b corresponding to the two sides of the ladder (right).

- Two species -> hyperfine states?
- Polar molecules?

Conclusions

- We have proposed a gauge-invariant approach for the quantum simulation of the abelian Higgs model.
- The tensor renormalization group formulation allows reliable calculations of the phase diagram and spectrum.
- Calculations of the entanglement entropy for the $O(2)$ model in the superfluid phase at increasing N_x are consistent with a CFT of central charge 1. Scaling of truncation (how to increase D_{bound} with the size) needs to be understood better.
- Calculations of the Polyakov loop at finite N_x and small gauge coupling shows an interesting behavior (finite volume deconfinement, related to the KT transition of the limiting $O(2)$ model). Nice data collapse at weak gauge coupling.
- We have proposed a Bose-Hubbard model that corresponds to the spin-1 version and proposed an implementation on optical lattices. We were able to match the spectra in the large U limit.
- Thanks!

3D gauge theories

A blocking procedure can be constructed by sequentially combining two cubes into one in each of the directions (PRD 88 056005)
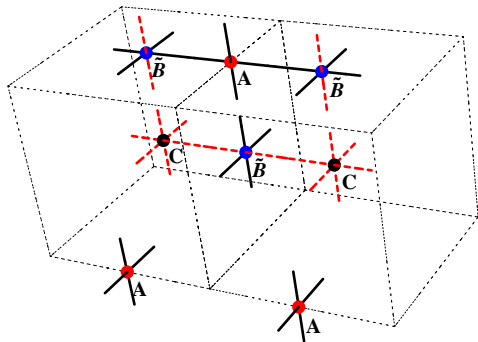
Other applications?

- Abelian Higgs model with a topological term
  Adding a topological term $S_{top} = \imath \frac{\Theta}{2\pi} \sum_x Im U_{\square,x}$ to the (1+1)D
  Abelian Higgs model, and in the limit $\kappa_\tau \gg \beta \gg \kappa_s$ as well as
  $\beta \gg \Theta$, we get:

$$H_{top} = H + \frac{\tilde{U}_P \Theta}{2\pi} \sum_i \bar{L}_i^z \tag{2}$$

- Abelian Higgs model in (2+1)D
  In the limiit $\kappa_\tau \gg \beta_\tau \gg \beta_s, \kappa_s$

$$H_{2+1} = H_2 - \frac{\beta_s}{2a} \sum_r (L_{r,\hat{x}}^+ L_{r+\hat{x},\hat{y}}^+ L_{r+\hat{y},\hat{x}}^- L_{r,\hat{y}}^- + h.c.) \tag{3}$$

where H_2 is the 2d version of the Hamiltonian obtained in (1+1)D
case, β_s is the gauge coupling in $x - y$ plane. To simulate the
quartic term, we need to go to the fourth order degenerate
perturbation theory for Bose Hubbard model.

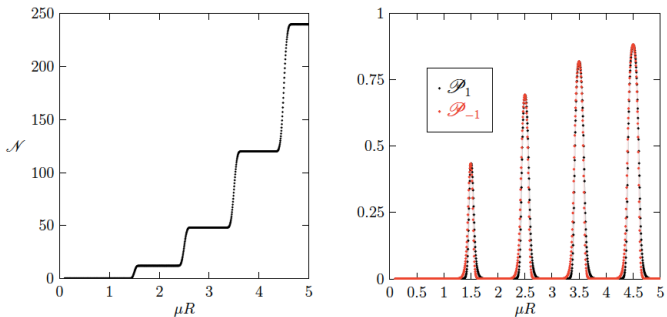# QCD with chemical potential on $S_1 \times S_3$

Figure 1: Quark number (Left) and Polyakov lines (Right) as a function of the chemical potential for QCD on $S^1 \times S^3$. (Right). $N = 3, N_f = 1, m = 0, \beta/R = 30$ (low T).

Figure: From: Simon Hands, Timothy J. Hollowood, Joyce C. Myers, arxiv 1012.0192, Lattice 2010.

Combining TRG and new perturbative methods?

- The divergence of QFT perturbative series can be traced to the large field configurations. For suitably chosen field cuts, converging perturbative series provide good approximation of results that can be obtained by independent numerical methods. The method can be combined with blocking for the hierarchical model. (YM, PRL 88, 141601 (2002)).

- In many of the TRG calculations, the microscopic tensor is constructed in terms of $I_n(\beta) = \frac{1}{2\pi} \int_{-\pi}^{\pi} d\theta e^{\beta \cos(\theta) + in\theta}$. In the known asymptotic expansions of the $I_n(\beta)$, one adds tails of integration to the compact range in order to get Gaussian integrals. Keeping the range of integration finite leads to converging weak coupling expansion (L. Li and YM PRD 71 054509 (2005)). Hopefully this can be connected to resurgence ideas.

- Understanding the connection between topology and the perturbative expansion for the 1D O(2) model on a lattice is easy (Poisson summation), but a challenging problem in 2D.

The transfer matrix $\mathbb{T}$ of the AHM

$$\mathbb{B}_{(m_1, m_2, \ldots m_{N_s})(m'_1, m'_2 \ldots m'_{N_s})} = t_{m_1}(2\kappa_\tau)\delta_{m_1, m'_1} t_{m_1}(\beta_{pl}) \times$$
$$t_{|m_1 - m_2|}(2\kappa_\tau)\delta_{m_2, m'_2} t_{m_2}(\beta_{pl}) t_{|m_2 - m_3|}(2\kappa_\tau) \ldots$$
$$t_{m_{N_s}}(\beta_{pl}) t_{m_{N_s}}(2\kappa_\tau)$$

Note that with this choice of open boundary conditions, the chemical potential has completely disappeared. If we had chosen different m's at the end allowing a total charge Q inside the interval, we would have an additional factor $\exp(\mu Q)$. We next define a matrix $\mathbb{A}$ as the product.

$$\mathbb{A}_{(m_1, m_2, \ldots m_{N_s})(m'_1, n'_2 \ldots m'_{N_s})} =$$
$$t_{|m_1 - m'_1|}(2\kappa_s) t_{|m_2 - m'_2|}(2\kappa_s) \ldots t_{|m_{N_s} - m_{N'_s}|}(2\kappa_s)$$

With these notations we can construct a symmetric transfer matrix $\mathbb{T}$. Since $\mathbb{B}$ is diagonal, real and positive, we can define its square root in an obvious way and write the transfer matrix as

$$\mathbb{T} = \sqrt{\mathbb{B}} \mathbb{A} \sqrt{\mathbb{B}}$$

The partition function

$$Z = (I_0(\beta_{pl})I_0(2\kappa_s)I_0(2\kappa_\tau))^V \mathrm{Tr}\left[\mathbb{T}^{N_\tau}\right]$$

Alternatively, we could diagonalize the symmetric matrix $\mathbb{A}$ and define the (dual) transfer matrix

$$\tilde{\mathbb{T}} = \sqrt{\mathbb{A}}\mathbb{B}\sqrt{\mathbb{A}}$$

The $\mathbb{A}$ and $\mathbb{B}$ matrices can be constructed by a recursive blocking method similar to what we discuss in PhysRevD.88.056005.

$$B'_{m_3 m_6 M(m_1,m_2)M'(m'_1,m'_2)} =$$
$$\sum_{m_4,m'_1} B_{m_3 m_4 m_1 m'_1} A^{(\tau)}_{m_4 m_5} B_{m_5 m_6 m_2 m'_2}$$

$$A'^{(s)}_{M(m_1,m_2)M'(m'_1,m'_2)} = A^{(s)}_{m_1 m'_1} A^{(s)}_{m_2 m'_2}$$
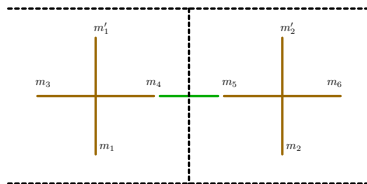
Graphical representation of blocking

Figure: Part of the construction of the blocked B' tensor. This shows the contraction of the B and $A^{(\tau)}$ tensors. The dashed lines are the links of the original lattice.

Figure: Graphical representation of the blocking of the A tensors. The vertical tensors are the $A^{(s)}$ and the dashed lines are the links of the original lattice.
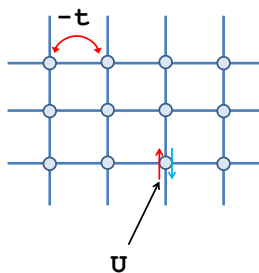
The Fermi-Hubbard model

Fermi-Hubbard model Hamiltonian:

$$H = -t \sum_{\langle i,j \rangle, \alpha} (c_{i,\alpha}^{\dagger} c_{j,\alpha} + h.c.) + U \sum_{i=1}^{N} n_{i\uparrow} n_{i\downarrow}$$

where t characterizes the tunneling between nearest neighboor sites and U controls the onsite Coulomb repulsion. These interactions can be approximately recreated with the atoms trapped in an optical lattice.

In the strong coupling limit ($U \gg t$) and at half-filling, Fermi-Hubbard $\sim$ spin-1/2 quantum Heisenberg

$$H = J \sum_{<\mathbf{ij}>} \mathbf{S_i} \cdot \mathbf{S_j} \quad \text{with} \ \ J = 4t^2/U$$

Using $\mathbf{S_i} = \frac{1}{2} f_{\mathbf{i}\alpha}^\dagger \sigma_{\alpha\beta} f_{\mathbf{i}\beta}$, the Heisenberg Hamiltonian becomes

$$H = \sum_{<\mathbf{ij}>} -\frac{1}{2} J f_{\mathbf{i}\alpha}^\dagger f_{\mathbf{j}\alpha} f_{\mathbf{j}\beta}^\dagger f_{\mathbf{i}\beta} + \sum_{<\mathbf{ij}>} J(\frac{1}{2} n_{\mathbf{i}} - \frac{1}{4} n_{\mathbf{i}} n_{\mathbf{j}})$$

A constraint must be imposed in order to recover the original Heisenberg model: $f_{\mathbf{i}\alpha}^\dagger f_{\mathbf{i}\alpha} = 1$.

The model has a local $SU(2)$ symmetry (Anderson et al.)

Baryons and Mesons (Fradkin et al.)

After a particle-hole transformation in the spin down operator

$$f_{\mathbf{i},\uparrow}, f_{\mathbf{i},\uparrow}^{\dagger} \to \Psi_{x,1}, \Psi_{x,1}^{\dagger}; \qquad f_{\mathbf{i},\downarrow}, f_{\mathbf{i},\downarrow}^{\dagger} \to \Psi_{x,2}^{\dagger}, \Psi_{x,2}$$

The Heisenberg Hamiltonian can be written as follows

$$H = \frac{J}{8} \sum_{x,\hat{\mathbf{i}}} [M_x M_{x+\hat{\mathbf{i}}} + 2(B_x^{\dagger} B_{x+\hat{\mathbf{i}}} + B_{x+\hat{\mathbf{i}}}^{\dagger} B_x)] - \frac{Jd}{4} \sum_x (M_x - \frac{1}{2})$$

The "meson" and "baryon" operators are as in lattice gauge theory:

$$M_x = \sum_{a=1,2} \Psi_{x,a}^{\dagger} \Psi_{x,a}$$

and

$$B_x = \sum_{a=1,2} \frac{\epsilon_{ab}}{2} \Psi_{x,a} \Psi_{x,a} = \Psi_{x,1} \Psi_{x,2}$$
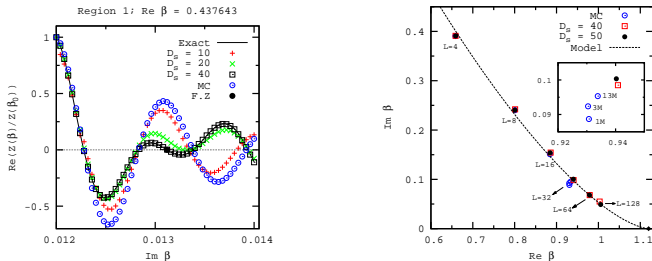
Figure: Left: the real part of the normalized partition function $\mathrm{Re}[Z(\beta)/Z(\beta_0)]$ for β near the Fisher zero $0.437643 + i0.01312$ (the big filled circle on the horizontal axis): result from the HOTRG with $D_s = 10, 20, 40$ ($D_s = 30$ result is not shown as it is close to the $D_s = 40$ case), MC, and exact solution. Right: zeros of XY model with linear size $L = 4, 8, 16, 32, 64, 128$ (from up-left to down-right) calculated from HOTRG with $D_s = 40, 50$ and zeros with $L = 4, 8, 16, 32$ from MC. The curve is a model for trajectory of the lowest zeros. Fit: $\mathrm{Im}\beta_z = 1.27986 \times (1.1199 - \mathrm{Re}\beta_z)^{1.49944}$.

Irrelevant directions can be slow: problem for small volumes. Finite size scaling (Fisher zeros)?
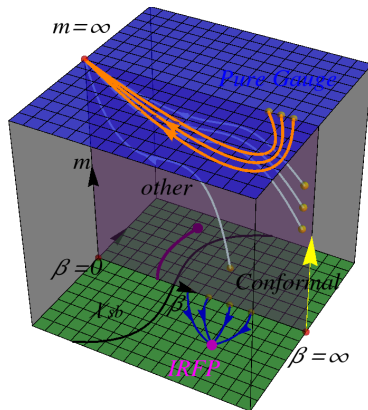

Figure: Schematic flows for $SU(3)$ with 12 flavors (picture by Yuzhi Liu).

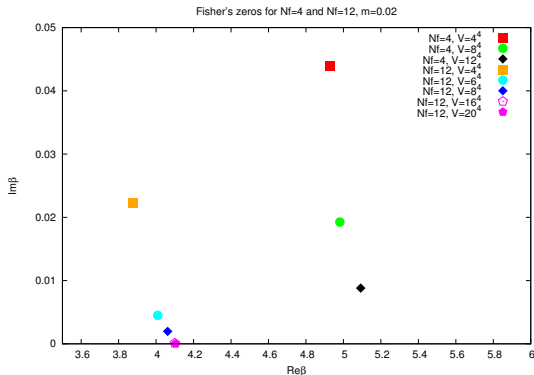# Fisher zeros for $SU(3)$ with $N_f = 4$ and 12 (Yuzhi Liu)

Fisher's zeros for Nf=4 and Nf=12, m=0.02

Figure: Zeros for $N_f = 4$ and $N_f = 12$ for L^4 lattices ($L = 16, 20$). 12 flavors pinch the real axis, the zeros scale like L^{-4} (first order) transtion.
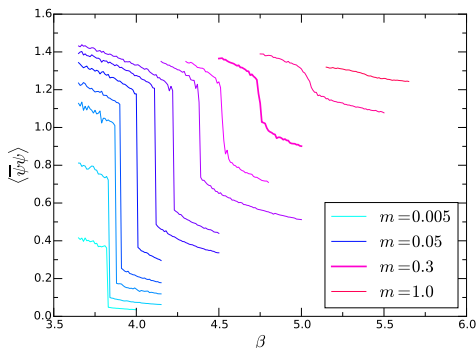
Figure: Unimproved HMC. Chiral condensate vs. $\beta = 6/g^2$ for increasing m, with Nf = 12, V = 4^4. The masses included (from left to right) are as follows: 0.0050, 0.0105, ... , 0.5000, 0.9999. Will the Fisher's zero pinch the real axis like L^{-2} (ν=1/2, mean field for a free scalar) instead of L^{-4} near the end point (for $m = m_c$)? Does first order scaling changes when $m \to 0$?